Frequency analysis and representation of slowly diffusing planetary solutions

Y. N. Fu, J. Laskar

HAL Id: hal-02276075
https://hal.sorbonne-universite.fr/hal-02276075v1

Submitted on 2 Sep 2019

Frequency analysis and representation of slowly diffusing planetary solutions[*]

Y. N. Fu[1] and J. Laskar[2]

[1] Purple Mountain Observatory, Chinese Academy of Sciences, 2 West Beijing Road, 210008 Nanjing, PR China
e-mail: fyn@pmo.ac.cn
[2] ASD/IMCCE, Observatoire de Paris, PSL University, CNRS, Sorbonne Université, 77 avenue Denfert-Rochereau, 75014 Paris, France
e-mail: laskar@imcce.fr

ABSTRACT

Context. Over short time-intervals, planetary ephemerides have traditionally been represented in analytical form as finite sums of periodic terms or sums of Poisson terms that are periodic terms with polynomial amplitudes. This representation is not well adapted for the evolution of planetary orbits in the solar system over million of years which present drifts in their main frequencies as a result of the chaotic nature of their dynamics.
Aims. We aim to develop a numerical algorithm for slowly diffusing solutions of a perturbed integrable Hamiltonian system that will apply for the representation of chaotic planetary motions with varying frequencies.
Methods. By simple analytical considerations, we first argue that it is possible to exactly recover a single varying frequency. Then, a function basis involving time-dependent fundamental frequencies is formulated in a semi-analytical way. Finally, starting from a numerical solution, a recursive algorithm is used to numerically decompose the solution into the significant elements of the function basis.
Results. Simple examples show that this algorithm can be used to give compact representations of different types of slowly diffusing solutions. As a test example, we show that this algorithm can be successfully applied to obtain a very compact approximation of the La2004 solution of the orbital motion of the Earth over 40 Myr ([−35 Myr, 5 Myr]). This example was chosen because this solution is widely used in the reconstruction of the past climates.

Key words. methods: numerical – celestial mechanics – ephemerides – planets and satellites: dynamical evolution and stability – chaos

1. Introduction

Before the computer age, long-term solutions for planetary orbits were derived by perturbation methods, and were obtained in the form of the sum of periodic terms. The first such solution was obtained by Lagrange (1782) and was later on improved by LeVerrier (1840, 1841), who took Uranus into account as well. These long-term solutions have been found to be of fundamental importance for the understanding of the past climate of the Earth, when it was understood that the changes of the orbit of the Earth also induce some change in its obliquity and in the insolation at the Earth surface (Milankovitch 1941; for a detailed review, see Laskar et al. 2004). With the advent of computers, two different approaches become possible. Computer algebra allowed extending the perturbation methods (e.g., Bretagnon 1974), and as computer speed increased, direct integrations of the full solar system become possible (Quinn et al. 1991; Sussman & Wisdom 1992). Instead, Laskar (1985, 1986, 1988) developed a mixed strategy in which an analytical averaging of the planetary equations by perturbation methods was obtained with dedicated computer algebra, followed by numerical integration of the averaged system. In order to compare the output of the numerical integrations with the quasi-periodic solutions of the perturbative meth-

ods, Laskar (1988) introduced the frequency analysis method that allows obtaining in a very efficient way a precise approximation of the numerical solution in quasiperiodic form (e.g., Laskar 2003).

One outcome of these computations was also to demonstrate that the solar system motion is chaotic (Laskar 1989, 1990). As a consequence, the solutions are not quasi-periodic, although they can be approximated by a quasi-periodic expression over a limited time of a few million years (Laskar 1988, 1990; Laskar et al. 2004).

We here derive a more adapted strategy for the slowly diffusing trajectories of a dynamical system that is very well suited to the construction of compact forms for the long-time behavior of planetary orbits. We introduce an algorithm that is derived from the frequency analysis to which a slow variation of the frequencies and amplitudes is added. By slowly diffusing solution, we mean a solution that while it experiences significant frequency drifts during the entire considered time interval is nearly quasi-periodic in time subintervals. Similar to the frequency analysis, a key step of our algorithm is to construct a frequency-dependent function basis on which the considered solution is decomposed.

After recalling some fundamental results of the frequency analysis, we consider in Sect. 2 a single-term model and show that it is possible to exactly recover its varying frequency as a function of time. This is important when the details of how a solution diffuses in the frequency space are of interest. To

---

construct a compact solution representation with a reasonably high precision, however, small flickers without significant cumulative effects can be smoothed out from a varying frequency. It is therefore preferable to use a model with a limited number of parameters, for instance, low-order polynomials, to approximate the frequency. To do so, we sample the averaged frequencies over a sliding time-interval. For a slowly diffusing solution, it is assumed that all fundamental frequencies can be sampled in this way using the algorithm called numerical analysis of fundamental frequencies (NAFF; e.g., Laskar 2003).

We design a general algorithm that represents a slowly diffusing solution in Sect. 3, where a frequency-dependent function basis is constructed based on the Chebyshev approximations of fundamental frequencies. The basis functions with significant but non-fundamental frequencies are generated according to the assumption that at any instant, a slowly diffusing solution is nearly quasi-periodic with the smoothed fundamental frequencies at that instant: all main frequencies are integral linear combinations of the fundamental frequencies. This effectively avoids the difficulties of determining the frequencies of long-period terms and/or groups of neighboring-period terms.

Two simple examples are given in Sect. 4. In the first example, a weakly dissipated system is considered, and the represented solution diffuses because of dissipation. In the second example, a Hamiltonian system of degree 1.5 is considered, and a solution starting from an obvious resonance overlap zone is represented. To show the flexibility of our algorithm in representing such a solution, we exclude all possible libration frequencies from the set of fundamental frequencies used in constructing the function basis.

Applications to the representation of ephemerides of the solar system bodies are provided in Sect. 5. As examples, we represent the eccentricity and inclination of the Earth as given by the long-term numerical solution La2004 (Laskar et al. 2004). For such a realistic solution, it is natural to take restrictions on the representation model from previous results into account, such as the important libration frequencies from numerical analysis (e.g., Laskar et al. 2004), so that the resulting representations can be as similar as possible to the physical model.

2. Frequency analysis and time-dependent frequencies

For a KAM solution (after Kolmogorov, Arnold, Moser) of a dynamical system (Kolmogorov 1954; Arnol'd 1963; Moser 1962), with fundamental frequency vector $\boldsymbol{\nu} = (\nu_1, \ldots, \nu_N) \in R^N$, where N is the number of degrees of freedom of the system, the motion of any given degree of freedom variable $z(t)$ can be described in complex form as

$$z(t) = \sum_{\boldsymbol{k} \in Z^N} a_{\boldsymbol{k}} e^{i\langle \boldsymbol{k}, \boldsymbol{\nu} \rangle t}, \tag{1}$$

where $\boldsymbol{k} = (k_1, \ldots, k_N)$ is the frequency index vector, $a_{\boldsymbol{k}}$ complex amplitude, and $\langle \cdot, \cdot \rangle$ denotes the usual inner product of two real vectors.

The NAFF algorithm was designed to numerically recover significant terms of Eq. (1) from a numerical sample set of $z(t)$, for example, an ephemeris obtained by numerical integration (Laskar 1988). However, the application of NAFF is not limited to numerically recovering KAM solutions. Actually, most of the relevant works concern frequency drifts. In particular, the variations in fundamental frequencies of the secular solar system over 200 Myr was used to study the chaotic behavior of the solar system (Laskar 1990).

We first briefly recall the theorem about the convergence of the NAFF algorithm (for the complete version with proof, see Laskar 2003). With a set of N appropriate variables, the complex function (1) describing a degree of freedom of an analytic KAM solution can be written as

$$z(t) = e^{i\nu_1 t} + \sum_{\boldsymbol{k} \in Z^N - (1,0,\ldots,0)} a_{\boldsymbol{k}} e^{i\langle \boldsymbol{k}, \boldsymbol{\nu} \rangle t} \quad (|a_{\boldsymbol{k}}| < 1), \tag{2}$$

where ν_1 is a fundamental frequency. We have then the following (e.g. Laskar 1999).

Theorem 1. Let ν_1^T be the value of $\sigma \in R$ that maximizes the function $\phi(\sigma) = |\langle z(t), e^{i\sigma t} \rangle_T^\chi|$, where $\chi = \chi(t/T) > 0$ is a weight function, and $\langle \cdot, \cdot \rangle_T^\chi$ the inner product of two complex functions of t defined as

$$\langle f(t), g(t) \rangle_T^\chi = \frac{1}{2T} \int_{-T}^{T} f(t)\bar{g}(t)\chi(t/T)\mathrm{d}t. \tag{3}$$

We then have $\lim_{T \to \infty} \nu_1^T = \nu_1$. □

Similar to the fundamental frequency ν_1, any other main frequency can be recovered by searching its neighborhood or R for the value of σ that maximizes $\phi(\sigma)$, defined with the remaining $z(t)$, that is, the original $z(t)$ minus the recovered terms.

A diffusion solution is then characterized by fundamental frequency variations (Laskar et al. 1992; Laskar 1993). To determine a varying frequency, we first consider the following simplest case,

$$f(t) = a(t)e^{i\int_0^t \nu(\tau)\mathrm{d}\tau}, \tag{4}$$

where $\nu(t)$ and $a(t) > 0$ are real integrable functions. Writing

$$\phi(\sigma(t)) = \left| \left\langle f(t), e^{i\int_0^t \sigma(\tau)\mathrm{d}\tau} \right\rangle_T^\chi \right| = \left| \frac{1}{2T} \int_{-T}^{T} a(t)e^{i\theta(t)}\chi(t/T)\mathrm{d}t \right|, \tag{5}$$

where $\theta(t) = \int_0^t (\nu(\tau) - \sigma(\tau))\mathrm{d}\tau$ belongs to C^0, the set of continuous function on R, we have the theorem below.

Theorem 2. For any given $T > 0$ and $\nu(t) \in C^0$, the functional $\phi(\sigma(t))$ has one and only one maximum in C^0, which is attained at $\sigma(t) \equiv \nu(t)$.

Proof. The right-hand side of Eq. (5) can be written as

$$\left| \frac{1}{2T} \int_{-T}^{T} \left(\sqrt{a(t)} \right)\left(\sqrt{a(t)}e^{i\theta(t)} \right)\chi(t/T)\mathrm{d}t \right| = \left| \left\langle \sqrt{a(t)}, \sqrt{a(t)}e^{-i\theta(t)} \right\rangle_T^\chi \right|.$$

Using the Cauchy–Bunyakovsky–Schwarz inequality[1], we can easily deduce from this formula that

$$\phi(\sigma(t)) \leq \left\| \sqrt{a(t)} \right\| \times \left\| \sqrt{a(t)}e^{-i\theta(t)} \right\| = \frac{1}{2T} \int_{-T}^{T} a(t)\chi(t/T)\mathrm{d}t,$$

where $\| \cdot \|$ denotes the norm induced by the inner product (3). Moreover, the equality is true if and only if $\sqrt{a(t)}$ and $\sqrt{a(t)}e^{-i\theta(t)}$ are linearly dependent, that is, when $\theta(t)$ is a constant. This constant is 0, since $\theta(0) = 0$ by definition. The above arguments imply that $\phi(\sigma(t))$ has a unique maximum attained at $\theta(t) \equiv 0$. Because $\nu(t)$ is continuous and the searched $\sigma(t)$ is also continuous, $\theta(t) \equiv 0$ is equivalent to $\sigma(t) \equiv \nu(t)$. We therefore conclude

---

[1] Given any two vectors f and g in an inner product space, the Cauchy–Bunyakovsky–Schwarz inequality writes $\langle f, g \rangle \leq \|f\| \times \|g\|$, where $\langle \cdot, \cdot \rangle$ denotes the inner product and $\| \cdot \|$ the induced norm. In addition, the equality is true if and only if f and g are linearly dependent.

for any given $T > 0$ that $\phi(\sigma(t))$ has one and only one maximum attained at $\sigma(t) \equiv \nu(t)$ □.

Theorem 2 implies that even in the case of a varying frequency, it is still possible to recover the frequency exactly, as a function of time. Now, we consider the following more general complex function:

$$f(t) = a_1(t)e^{i\int_0^t \nu_1(\tau)d\tau} + \sum_{\boldsymbol{k} \in Z^N - (1,0,\dots,0)} a_{\boldsymbol{k}}(t)e^{i(\theta_{\boldsymbol{k}} + \int_0^t \langle \boldsymbol{k}, \nu(\tau) \rangle d\tau)}, \qquad (6)$$

where $a_1(a_{\boldsymbol{k}}) \in S_a$ with S_a a subspace of real function space, $\theta_{\boldsymbol{k}} \in R$, and $\{\nu_n\}_{n=1}^N \in S_\nu$ with S_ν a linear subspace of the real integrable function space. As an extension of Eq. (2), this function inherits an important time-varying character of Eq. (2), that is, all phase increments are described by a single fundamental frequency vector $\nu(t)$. We make the heuristic assumption that under suitable conditions, a similar result as for Theorem 1 holds for a more general expression with varying frequencies as in Eq. (6).

Assumption. If $\|\nu_1^T - \nu_1\|$ is sufficiently small, where $\nu_1^T \in S_\nu$ and $\| \cdot \|$ is an appropriately defined T-dependent norm (e.g., the one induced by the inner product (3)), and $\sigma(t) = \nu_1^T(t)$ (locally) maximizes the functional $\phi(\sigma) = |\langle f(t), e^{i\int_0^t \sigma(\tau)d\tau} \rangle_T^\chi|$, then $\lim_{T \to \infty} \nu_1^T(t) = \nu_1(t)$.

3. Representation of slowly diffusing solutions

From now on, we restrict ourselves to slowly diffusing solutions of an ordinary differential equation system obtained by slightly perturbing an integrable Hamiltonian system. We denote by $(I, \theta) = \{I_n, \theta_n\}_{n=1}^N$ the action-angle variables of the integrable Hamiltonian system, which is used to express the ephemeris of a diffusing solution $\{z_n(t) \equiv I_n(t)e^{i\theta_n(t)}\}_{n=1}^N$.

3.1. Representation procedure

We start from a sample set of $\{z_n(t)\}_{n=1}^N$. We assume that the samples are given at grid points from t_0 to t_1 with fixed time step h, which is much smaller than the minimum of the fundamental periods. In accordance with the condition of slow diffusion, we assume that the solution is close to quasi-periodic in the time subintervals (of $[t_0, t_1]$) described below, with a length far exceeding the maximum of the fundamental periods. These roughly stated preconditions are required because we use NAFF algorithm to estimate the changing fundamental frequencies.

As the first step, we apply the NAFF algorithm to obtain fundamental frequency samples. For each given degree (n), this algorithm is applied to $z_n(t)$ samples over evenly spaced time-subintervals $\{[\tau_\lambda - \frac{d}{2}, \tau_\lambda + \frac{d}{2}]\}_{\lambda=1}^\Lambda$ of $[t_0, t_1] = [\tau_1 - \frac{d}{2}, \tau_\Lambda + \frac{d}{2}]$. For each of these subintervals, the first recovered frequency is taken as the averaged value of the fundamental frequency ν_n over the same subinterval. The N averaged fundamental frequencies obtained in this way are then taken as the instant frequencies at τ_λ, resulting in the fundamental frequency samples $\{\tau_\lambda, \nu_n(\tau_\lambda)\}_{\lambda=1}^\Lambda, n = 1, \dots, N$.

Second, we fit for each given degree the frequency samples to a Chebyshev expansion valid on $[\tau_1, \tau_\Lambda]$,

$$\nu_n(t) = \sum_{m=0}^{M_n} c_{m,n} T_m(x) \qquad (n = 1, \dots, N), \qquad (7)$$

where $c_{m,n} \in R$ is a Chebyshev coefficient, $x = \frac{2(t-\tau_1)}{(\tau_\Lambda - \tau_1)} - 1 \in [-1, 1]$ a normalized time, and $T_m(x)$ is the Chebyshev

polynomial[2] of degree m. We then numerically construct a frequency-dependent function basis B (see the next subsection), on which the considered solution is decomposed.

The final step, that is, decomposing $z_n(t)$ on B, is the same as that of the NAFF algorithm (Laskar 1999), except for the searched function bases for significant terms. The function bases are $\{e^{i\omega_k t}, \omega_k \in R\}$ for NAFF and B for the procedure described here.

3.2. Representation model

By variation of parameters, Eq. (1) becomes

$$z_v(t) = \sum_{\boldsymbol{k} \in Z^N} a_{\boldsymbol{k}}(t)e^{i\int_0^t \langle \boldsymbol{k}, \nu(\tau) \rangle d\tau}. \qquad (8)$$

Now, let

$$\hat{Z}^N = \{k_n : |k_n| \leq K_n \in Z^+\}_{n=1}^N \qquad (9)$$

be a truncated set of the frequency index vector $\boldsymbol{k}$. For each $\boldsymbol{k} \in \hat{Z}^N$, let

$$a_{\boldsymbol{k}}(t) \approx \sum_{l=0}^{L_{\boldsymbol{k}}} \widetilde{a_{l,\boldsymbol{k}}} \, T_l(x(t)) \qquad (10)$$

be a Chebyshev expansion of the amplitude valid on $[\tau_1, \tau_\Lambda]$, where $\widetilde{a_{l,\boldsymbol{k}}} \in C$. These lead us from Eq. (8) to the following representation model of $z_v(t)$:

$$z_v(t) \approx \sum_{\boldsymbol{k} \in \hat{Z}^N} \sum_{l=0}^{L_{\boldsymbol{k}}} \widetilde{a_{l,\boldsymbol{k}}} \, T_l(x(t))e^{i\int_0^t \langle \boldsymbol{k}, \nu(\tau) \rangle d\tau}. \qquad (11)$$

From the Chebyshev approximations of the fundamental frequencies, it is easy to obtain by integration the Chebyshev expansion representing the phase increment associated with the frequency $\langle \boldsymbol{k}, \nu(\tau) \rangle$, from the value, as is preferred, at the middle of the time interval $[\tau_1, \tau_\Lambda]$,

$$\int_{(\tau_1 + \tau_\Lambda)/2}^t \langle \boldsymbol{k}, \nu(\tau) \rangle d\tau = \varphi_{0\boldsymbol{k}} + \varphi_{\boldsymbol{k}}(t) \quad (\boldsymbol{k} \in \hat{Z}^N), \qquad (12)$$

where $\varphi_{0\boldsymbol{k}} \in R$, and $\varphi_{\boldsymbol{k}}(t)$ gathers all Chebyshev polynomials of degree larger than 0. With $\varphi_{0\boldsymbol{k}}$ and $\varphi_{\boldsymbol{k}}(t)$, Eq. (11) can be written as

$$z_v(t) \approx \sum_{\boldsymbol{k} \in \hat{Z}^N} \sum_{l=0}^{L_{\boldsymbol{k}}} a_{l,\boldsymbol{k}} \, T_l(x(t))e^{i\varphi_{\boldsymbol{k}}(t)}, \qquad (13)$$

where $a_{l,\boldsymbol{k}} = \widetilde{a_{l,\boldsymbol{k}}}e^{i\varphi_{0\boldsymbol{k}}} \in C$ is simply the coordinate of $z_v(t)$ when it is decomposed on the function basis

$$B = \{b_{l,\boldsymbol{k}}\} = \{T_l(x(t))e^{i\varphi_{\boldsymbol{k}}(t)}\}. \qquad (14)$$

For the obtained representation, it should be noted that although we decompose a solution on the basis B, and correspondingly, express its representation by Eq. (13), $\varphi_{\boldsymbol{k}}(t)$ is not used to specify the representation. $\{\nu_n(t)\}_{n=1}^N$ is used instead. In other words, the representation is specified by the coordinates $a_{l,\boldsymbol{k}}$, and the Chebyshev coefficients of $\{\nu_n(t)\}_{n=1}^N$. This choice is made for the following two reasons. One is that the representation could otherwise be unnecessarily cumbersome. The other

---

[2] The explicit expressions of $T_m(x)$ up to $m = 15$ are given in Table A.1.

Table 1. Summary of procedure parameters.

	Meaning	Venue
M_n	Degree of the polynomial approximating the nth fundamental frequency	(7)
K_n	Maximum index number associated with the nth fundamental frequency	(9)
L_k	Degree of the polynomial approximating the amplitude with index $\boldsymbol{k}$	(10)
J	Maximum number of representation terms	
δ	Absolute truncation error	(15)
δ_r	Relative truncation error	(16)

reason is that from the Chebyshev coefficients of $\{v_n(t)\}_{n=1}^N$, those of $\varphi_k(t)$ can be easily obtained according to Eq. (12). Here, we also recall that the solution representation, because of its dependence on the Chebyshev approximations of $v_n(t)$ and $a_k(t)$, is valid on $[\tau_1, \tau_\Lambda]$ rather than $[t_0, t_1]$.

To complete the description of the representation model, we point out that the integers $\{M_n, K_n\}_{n=1}^N$ and $\{L_k\}_{k \in \hat{Z}^N}$, introduced in Eqs. (7), (9), and (10), respectively, are necessary parameters for defining a particular representation procedure. Of course, the number of these parameters can be reduced by requiring that some or all of these parameters take the same sufficiently high value, for instance, $L_k = L$ for all $\boldsymbol{k} \in \hat{Z}^N$, at the price of unnecessarily increasing the basis dimension. Another important point to mention is that to terminate the procedure, the maximum number of representation terms (J) and/or the required precision has to be set beforehand. The required precision is specified by using either the absolute truncation error δ or the relative truncation error δ_r. Correspondingly, the procedure is terminated if

$$\|z - z_v\| < \delta \qquad (15)$$

or

$$\|z - z_v\|/\|z\| < \delta_r, \qquad (16)$$

where the module $\| \cdot \|$ is induced by the inner product (3) with prescribed $\chi \equiv 1$. In the following, these parameters, as summarized in Table 1, are referred to as procedure parameters.

4. Examples

In the following two subsections, we illustrate our representation procedure with two slowly diffusing solutions, of which one diffuses as a result of a dissipative perturbation, and the other as a result of its chaotic nature. In order to illustrate the convergence property of this procedure, it is convenient to write the resulting representation with a single term index, that is,
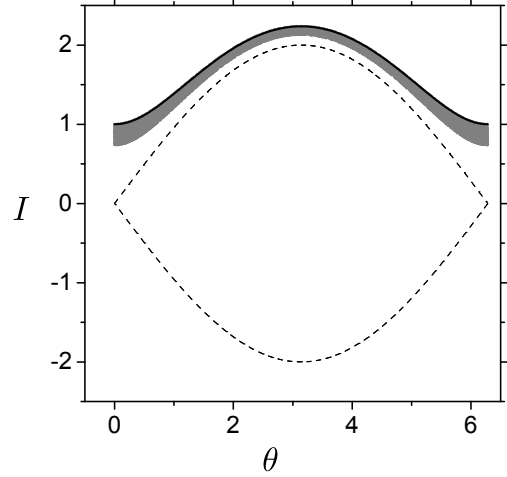
$$z_v(t) = \sum_{j=1}^J z_j(t) \equiv \sum_{j=1}^J a_j T_{l(j)}(x(t)) e^{i\varphi_{k(j)}(t)}, \qquad (17)$$

where the terms are arranged in the same order as they are obtained in the procedure, which roughly corresponds to the order of decreasing $|a_j|$.

4.1. Example of a dissipated solution

Consider the following weakly dissipated system:

$$\frac{d^2\theta}{dt^2} = \sin(\theta) - \varepsilon \frac{d\theta}{dt}, \qquad (18)$$

Fig. 1. Phase trajectory of the dissipated solution specified by Eqs. (18)–(20). Also shown is the phase orbit of the unperturbed pendulum system, namely (Eq. (18)) with $\varepsilon = 0$, which passes through the initial phase point of the dissipated solution. The dashed line depicts the separatrix of the unperturbed pendulum.
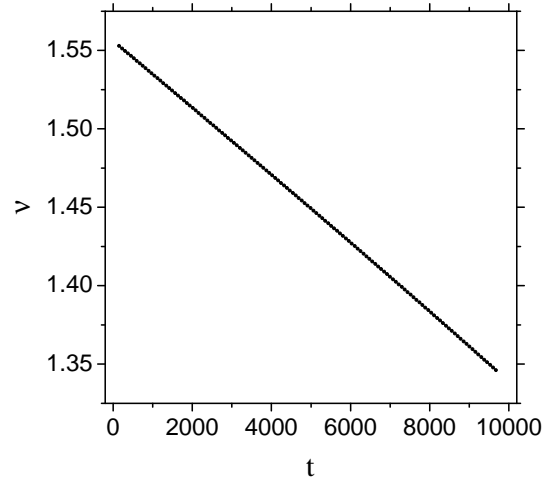
Fig. 2. Change of the fundamental frequency $v(t)$ of the dissipated solution specified by Eqs. (18)–(20). Also shown is a Chebyshev approximation of $v(t)$.

where

$$\varepsilon = 10^{-5}. \qquad (19)$$

If we nullify the dissipative term $-\varepsilon\frac{d\theta}{dt}$ in Eq. (18), the system is a simple pendulum with Hamiltonian $H_0(I) = \frac{I^2}{2} + \cos(\theta)$, where $I = \dot{\theta}$. Take as an example the solution $z(t) \equiv I(t)e^{i\,\theta(t)}$ of Eq. (18) with the following initial conditions:

$$t_0 = 0, \theta_0 = 0, I_0 = 1. \qquad (20)$$

Because of the dissipative perturbation, the phase orbit starting from (θ_0, I_0) gradually decays away from the unperturbed orbit passing through the same phase point. This dissipation effect is significant in the long run, as is shown in Fig. 1.

As a solution of a system of 1 degree of freedom with a dissipative perturbation, the decaying $z(t)$ has a changing fundamental frequency v, which inherits the characteristic frequency of the unperturbed system and varies as the solution decays.

Table 2. Coefficients of the Chebyshev expansion $\sum_{m=0}^{9} c_m T_m(x(t))$ approximating $\nu(t)$, the changing fundamental frequency of the dissipated solution specified by Eqs. (18)–(20).

m	c_m
0	$+1.450265 \times 10^{0}$
1	-1.032502×10^{-1}
2	-7.924442×10^{-4}
3	-1.163806×10^{-4}
4	-7.914948×10^{-6}
5	-6.369786×10^{-7}
6	-5.975314×10^{-8}
7	-3.609371×10^{-9}
8	$+1.771340 \times 10^{-9}$
9	$+8.159405 \times 10^{-9}$

Table 3. Leading 10 terms of Eq. (25), a representation of the dissipated solution $z(t)$ specified by Eqs. (18)–(20), which is obtained with $\{M, K, L, \delta_r\} = \{9, 10, 9, 10^{-5}\}$.

j	$l(j)$	$k(j)$	$\text{Arg}(a_j)$	$|a_j|$
1	0	1	-1.431544	1.378074489
2	0	2	0.278103	0.622837454
3	0	3	1.987348	0.159698128
4	1	1	1.748566	0.116187680
5	0	4	-2.587002	0.032622276
6	0	-1	-1.709654	0.017747854
7	1	2	0.133848	0.028210547
8	1	3	1.931736	0.027791194
9	0	5	-0.878547	0.005904572
10	1	4	-2.628911	0.009823726

4.2. Practical implementation

By numerical integration, an ephemeris of $z(t)$ is obtained at $\{t_i = ih : i = 0, \ldots, 65535, h = 0.15\}$. We then apply NAFF to 129 evenly spaced time subintervals with length $d = 2048\,h$ and midpoints $\{\tau_\lambda = \frac{d}{2} + 496(\lambda - 1)h\}_{\lambda=1}^{129}$, respectively, to obtain a sample set of the changing frequency, $\{\tau_\lambda, \nu(\tau_\lambda)\}_{\lambda=1}^{129}$. This frequency sample set is shown in Fig. 2. We also show a Chebyshev expansion approximating $\nu(t)$. This expansion is of degree 9 and is expressed as

$$\nu(t) \approx \sum_{m=0}^{9} c_m T_m(x) \quad \text{with} \quad x = \frac{2(t - \tau_1)}{\tau_{129} - \tau_1} - 1, \tag{21}$$

where the Chebyshev polynomials $T_m(x)$ are listed in Table A.1 and x is the time after normalization from $[\tau_1, \tau_{129}]$ to $[-1, 1]$. The values of the coefficients $\{c_m\}_{m=0}^{9}$ are given in Table 2.

We write the Chebyshev expansion approximating the phase increment, from the value at $x = 0$ or $t = \frac{\tau_1 + \tau_{129}}{2}$, associated with ν in two parts,

$$\int_{(\tau_1 + \tau_{129})/2}^{t} \nu(\tau)\mathrm{d}\tau = \varphi_0 T_0(x) + \varphi(x) \quad \text{with} \quad x = \frac{2(t - \tau_1)}{\tau_{129} - \tau_1} - 1, \tag{22}$$

where φ_0 is a real constant and

$$\varphi(x) = \frac{\tau_{129} - \tau_1}{2} \sum_{m=1}^{10} C_m T_m(x) \quad \text{with} \quad x = \frac{2(t - \tau_1)}{\tau_{129} - \tau_1} - 1 \tag{23}$$
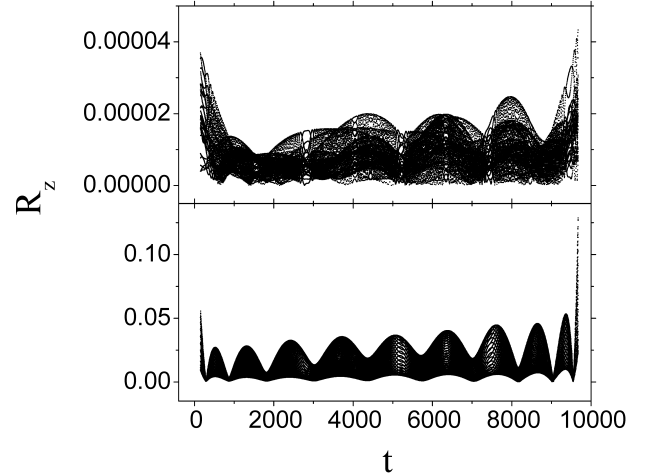
Fig. 3. Errors of two different representations of the dissipated solution specified by Eqs. (18)–(20). In the case of the upper panel, our representation procedure is terminated with a 37-term representation, because this representation reaches the precision requirement $\delta_r = 10^{-5}$. In the case of the lower panel, with slightly larger error in the frequency approximation, the representation is about 4 orders less precise, though the number of representation terms is increased to 150.
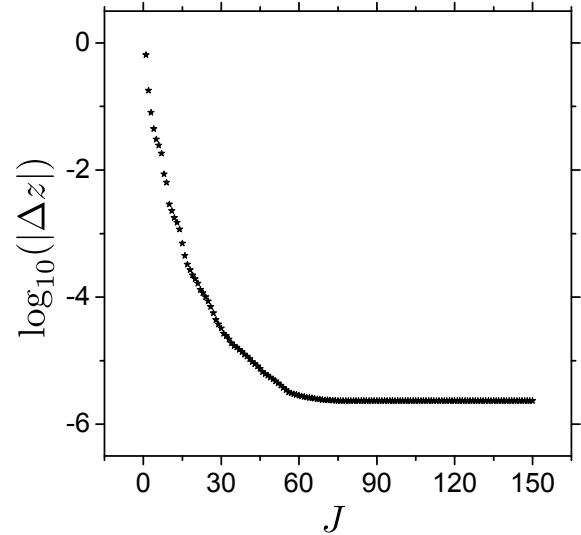
Fig. 4. Convergence property of the procedure of representing the dissipated solution specified by Eqs. (18)–(20). The residual of the representation is plotted against the number J of representation terms, where other procedure parameters are fixed as $\{M, K, L\} = \{9, 10, 9\}$.

gathers all Chebyshev polynomials of degree larger than 0. In Eq. (23), $\frac{\tau_{129} - \tau_1}{2}$ is the time-scaling factor, and[3], with $c_{10} = c_{11} = 0$,

$$C_m = \begin{cases} \frac{2c_0 - c_2}{2} & (m = 1), \\ \frac{c_{m-1} - c_{m+1}}{2m} & (m = 2, \ldots, 10). \end{cases} \tag{24}$$

This completes the determination of $\varphi(x)$, which is used in the following. Although the constant φ_0 is not used in the following, it can be easily determined as $\varphi_0 = -\varphi(0)$ because the phase increment (22) is 0 at $t = \frac{\tau_1 + \tau_{129}}{2}$ or $x = 0$.

With procedure parameters $\{M, K, L, \delta_r\} = \{9, 10, 9, 10^{-5}\}$, we obtain a 37-term representation,


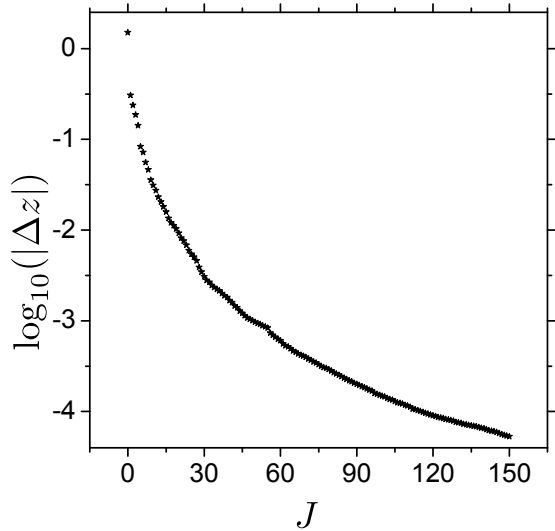3 For the general case, see Eq. (A.7).
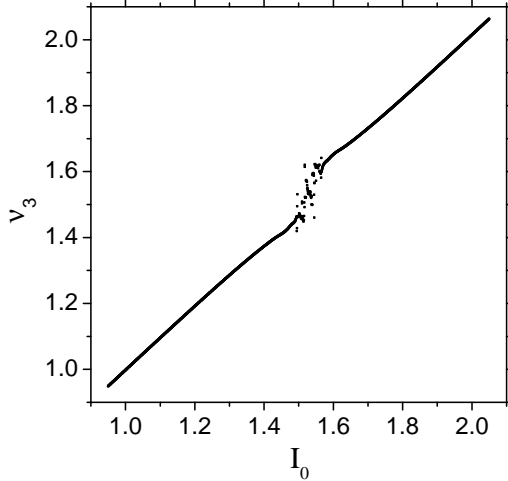
Fig. 5. Fundamental frequency map of the system specified by Eqs. (26) and (27). In the chaotic zone formed by resonance overlap lies the phase point $(\theta_0, I_0) = (0, 1.535)$, which will be chosen as the initial phase point of the considered chaotic solution.
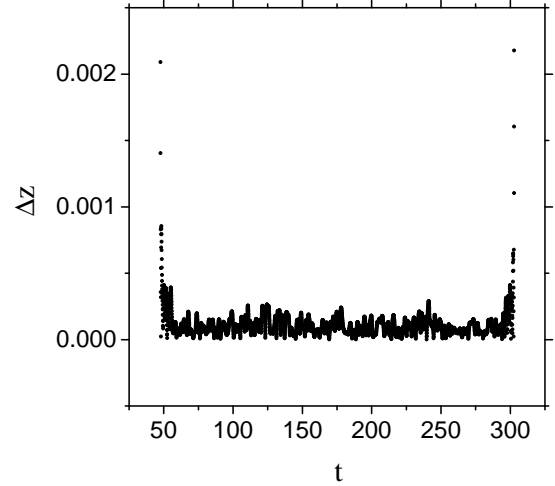
Fig. 7. Error of a 100-term representation of the chaotic solution specified by Eqs. (26)–(28). This representation is obtained with $\{M_1, M_2, M_3, K_1, K_2, K_3, L_k, J\} = \{0, 0, 9, 10, 10, 10, 9, 100\}$.
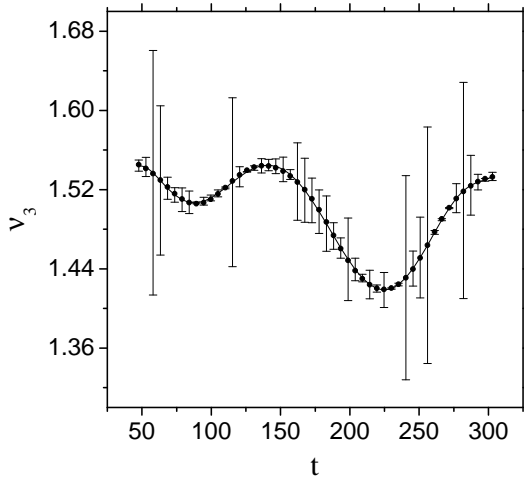
Fig. 6. Change of fundamental frequency $\nu_3(t)$ of the chaotic solution specified by Eqs. (26)–(28). The samples of this frequency are computed by applying NAFF algorithm over a sliding time-interval, and the errors are estimated as their respective differences from the frequencies of the quasi-periodic approximation of the solution over the same sliding time interval. Also shown is a Chebyshev appoximation of $\nu_3(t)$.

$$z_{37}(t) = \sum_{j=1}^{37} a_j T_{l(j)}(x) e^{i\varphi_{k(j)}(x)} \quad \text{with} \quad x = \frac{2(t - \tau_1)}{\tau_{129} - \tau_1} - 1, \quad (25)$$

of the solution $z(t)$, where $T_{l(j)}(x)$ is the Chebyshev polynomial of degree $l(j)$, and $\varphi_{k(j)}(x) = k(j)\varphi(x)$ the phase increment associated with the frequency $k(j)\nu$. The data needed for specifying the first ten representation terms are given in Table 3.

We now discuss how the procedure parameters affect the precision of the resulting representation. For this, we first consider a 150-term representation obtained by resetting $M = 1$. This resetting introduces only a small discrepancy in $\nu(t)$ because $|c_m/c_0| < 6 \times 10^{-4}$ for $m > 1$. The precision of this representation is several orders less precise than the previous one. As seen by comparing the two panels of Fig. 3, this is because the whole considered time interval is long, and the small discrepancy in $\nu(t)$ can accordingly result in significant phase errors. On the other hand, however, the fact that there is no term with either $|k| > 8$ or $l > 4$ in the 37-term representation indicates that

Fig. 8. Convergence property of the procedure of representing the chaotic solution specified by Eqs. (26)–(28). The residual of representation is plotted against the number J of representation terms. The other procedure parameters are fixed as $\{M_1, M_2, M_3, K_1, K_2, K_3, L_k\} = \{0, 0, 9, 10, 10, 10, 9\}$.

the representation model practically converges with respect to K and L. Our representation procedure also converges rapidly with respect to J. This is illustrated in Fig. 4, for which the procedure parameters excluding J are fixed as $\{M, K, L\} = \{9, 10, 9\}$.

4.3. Example of chaotic solutions of Hamiltonian system
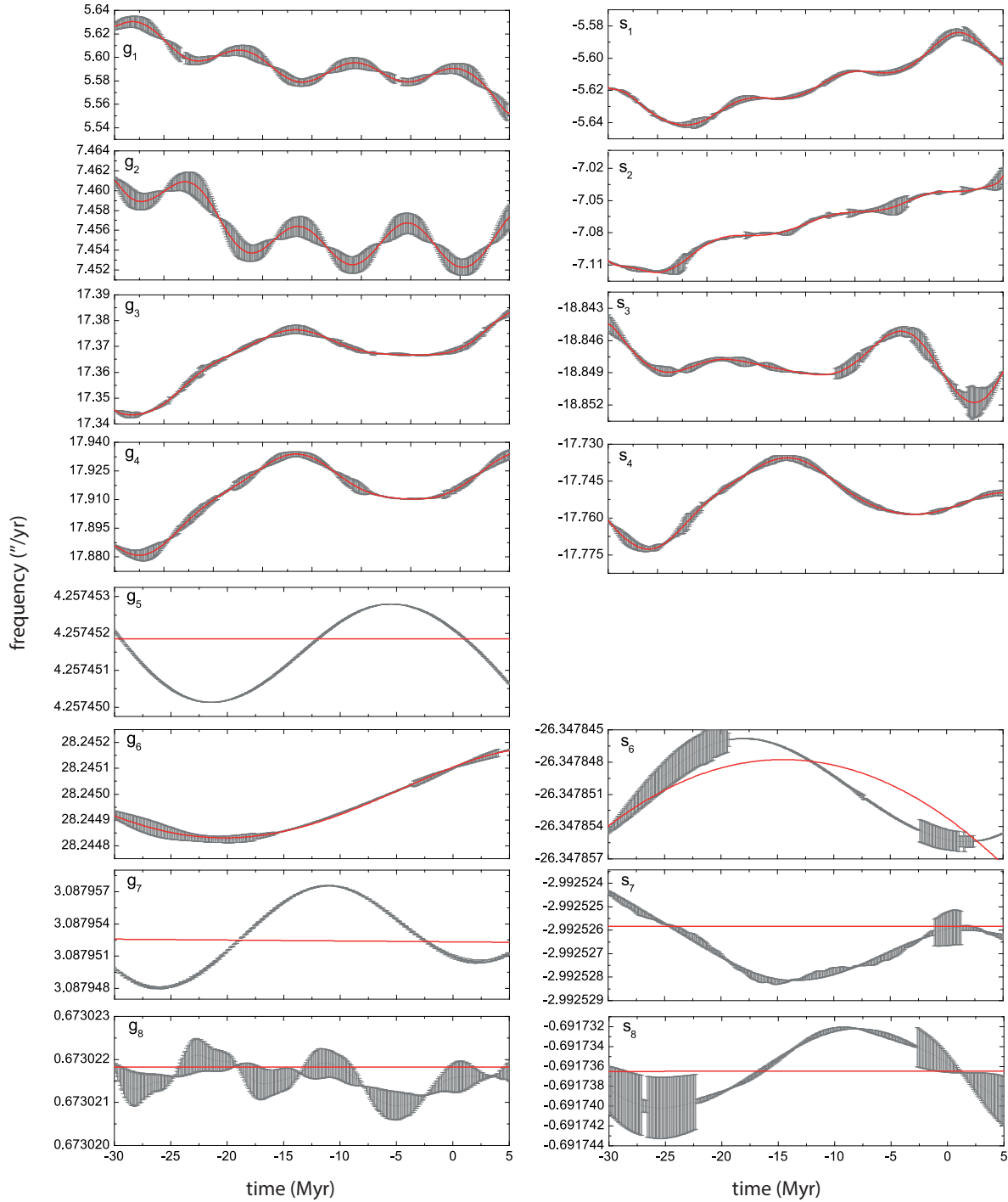
We consider the following Hamiltonian system:

$$H(I, \theta, t) = \frac{I^2}{2} + \varepsilon \cos(\theta)[1 + \cos(\nu_1 t) + \cos(\nu_2 t)], \quad (26)$$

where

$$\varepsilon = 5 \times 10^{-3}, \nu_1 = 1.5, \nu_2 = \frac{\pi}{2}. \quad (27)$$

A solution of this system has three fundamental frequencies. The first two are the forcing frequencies ν_1 and ν_2, which are

Fig. 9. Variations of major fundamental frequencies of the solar system over the time interval from -35 Myr to 5 Myr with origin at J2000. These frequencies (in arcsec yr^{-1}) are computed by applying the NAFF algorithm to the proper modes of the secular solar system associated with major planets. The errors in the resulting frequency samples are estimated as the difference between the frequencies computed respectively from the original ephemeris and its quasi-periodic approximation. Also shown in this figure are the Chebyshev approximations of these varing fundamental frequencies (red curves), which are specified in Table A.2.

non-commensurable. The other, denoted as ν_3, can be approximated in a similar way as in the previous subsection.

From the analysis of the frequency map (e.g., Laskar 1999), defined as $I_0 \to \nu_3$ with $\theta_0 = 0$ and shown in Fig. 5, we know that the phase point

$$t_0 = 0, \theta_0 = 0, I_0 = 1.535 \tag{28}$$

lies in a chaotic zone formed by resonance overlap, and the solution $z(t)$ starting from this point is chaotic.

An ephemeris of $z(t)$ is obtained by the symplectic integrator SBABc4 (Laskar & Robutel 2001) at $\{t_i = ih : i = 0, \ldots, 4095, h = 0.186058\}$. We then apply NAFF to 129 evenly spaced time intervals with length $d = 512 h$ and midpoints $\{\tau_\lambda = \frac{d}{2} + 28(\lambda - 1)h\}_{\lambda=1}^{129}$. This gives the sample set $\{\tau_\lambda, \nu_{3,\lambda}\}_{\lambda=1}^{129}$, partly shown in Fig. 6 together with a Chebyshev approximation. It should be noted that there are two intrinsically different error sources in this way of approximating a changing frequency. One error source is related to the NAFF process that gives the samples
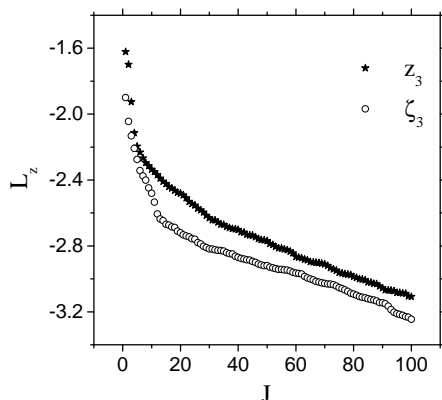
Fig. 10. Convergence property of the two representation procedures leading to the 100-term representations of $z_3(t)$ and $\zeta_3(t)$. The residual of the representation is plotted against the number J of the representation terms.

of the frequency, while the other is related to the fitting process that leads to a Chebyshev approximation of the frequency. Accordingly, we consider the Chebyshev approximation as sufficiently good if it deviates from the frequency sample set by much less than the sample uncertainties. As shown in Fig. 6, this requirement can be met with a Chebyshev polynomial of degree $M_3 = 9$.

Test calculations show that our representation procedure cannot lead to an acceptable representation of the solution on the whole sampling time-interval. There are two possible reasons for this.

The most intrinsic reason would be that our solution experiences passages into or out of resonance zones. Such a passage is associated with a shift between circulation and libration of the corresponding resonance angle, and accordingly, with occurrence or disappearance of certain terms. If some of these terms are significant enough in the whole considered time interval (τ_1, τ_{129}), then there would be no way to obtain any acceptable non-piecewise representation. Therefore, we restrict ourselves to the shorter time interval (τ_1, τ_{50}).

Another possible reason is that there are one or more significant libration frequencies, which are not taken into consideration when we generate the function basis B. While it is easy to make a necessary extension of B in order to include known libration frequencies (see Sect. 5), it is not that straightforward to identify and sample these frequencies (Laskar 1990). To show the flexibility of our algorithm, we do not search for any libration frequency and make the corresponding extension of B. The flexibility arises because when we choose reasonably high values of our procedure parameters K_n, then the resulting set of frequencies would be dense enough over a large frequency interval, in the sense that every important libration frequency is not far from at least one element of the frequency set.

Setting the procedure parameters as

$$\{M_1, M_2, M_3, K_1, K_2, K_3, L_k, J\} = \{0, 0, 9, 10, 10, 10, 9, 100\},$$

we obtain a 100-term representation of our solution. Figure 7 shows that the errors of this representation are typically smaller than $10^{-4}I_0$. Figure 8 also illustrates, in the same way as in the previous subsection, the convergence property of the representation procedure.

5. Application to planetary ephemerides

Numerical integration is now an efficient way of constructing ephemerides of the solar system bodies with high precision.

For practical applications, however, it can be useful to represent these discrete solutions analytically, and thus represent them in a continuous way.

These representations can be made in the form of segmented Chebyshev expansions, like those that represent the classical planetary ephemerides as INPOP (e.g., Fienga et al. 2008), or other generally applied approximation models without physical basis. A drawback of these representations is that they require large amounts of data. In order to obtain compact representations, Chapront (1995) used a model of Poisson series with fixed main frequencies that were obtained with the NAFF algorithm. Although this model already involves some long-term or long-period-term effects by allowing Poisson terms and therefore works well with planetary ephemerides of five outer planets over a few hundred years, it does not take the frequency drifts into consideration and cannot be used over millions of years.

The frequency drifts are important over a few tens of million years, as shown by Laskar (1990). The algorithm developed here is therefore expected to be more appropriate in representing ephemerides spanning this long time-interval. It is thus interesting to test whether our algorithm can be used to represent the long-term numerical solution of major solar system bodies over this long timescale (e.g., Laskar et al. 2004). For this, we applied our algorithm to the eccentricity and inclination variables of the Earth, that is,

$$z_3 = e_3 \exp(i\varpi_3) \quad \text{and} \quad \zeta_3 = \sin(i_3/2) \exp(i\Omega_3). \qquad (29)$$

To be more precise, e_3 and i_3 are the eccentricity and inclination, respectively, of the instantaneous orbit of the Earth-Moon barycenter, and ϖ_3 and Ω_3 are the longitudes of the perihelion and of the node of the same orbit with respect to the fixed J2000.0 equatorial reference system, respectively.

The chaotic behavior of the terrestrial orbit certainly limits the time span over which this orbit can be precisely determined, but z_3 and ζ_3 from La2004 are reliable and precise at least over the time span $[-35\,\text{Myr}, +5\,\text{Myr}]$, see Laskar et al. (2011). Therefore, we restricted our representations to this time span. Test calculations showed that our algorithm can lead to compact and precise representations for both degrees of freedom. With different procedure parameters, the resulting representations contain very different terms. This confirms the flexibility of our algorithm.

In order to give representations as physical as possible, we resorted to the knowledge we have for the solution. Following Laskar et al. (2004), we computed the fundamental frequencies of the secular solar system by applying the NAFF algorithm over time intervals of length 20 Myr for the proper modes $(z_1^{\bullet}, \ldots, z_4^{\bullet}, \zeta_1^{\bullet}, \ldots, \zeta_4^{\bullet})$, and 50 Myr for the proper modes $(z_5^{\bullet}, \ldots, z_8^{\bullet}, \zeta_5^{\bullet}, \ldots, \zeta_8^{\bullet})$[4]. From $-35\,\text{Myr}$ to $5\,\text{Myr}$ with a step 0.1 Myr, we generated the samples of the fundamental frequencies $(g_1, \ldots, g_8, s_1, \ldots, s_8)$ corresponding to these proper modes. The resulting nominal value of s_5 is about 0.00000015 arcsec yr^{-1}. The other frequency samples are shown in the panels of Fig. 9, where the errors are estimated as the difference between the values of a frequency computed from the associated ephemeris and its quasi-periodic approximation. We also show in this figure the Chebyshev approximations of these fundamental frequencies. All of these Chebyshev approximations, the coefficients of which are listed in Table A.2, were obtained by truncating those of degree 15. The

---

[4] See Laskar (1990) for the definition of the proper modes.
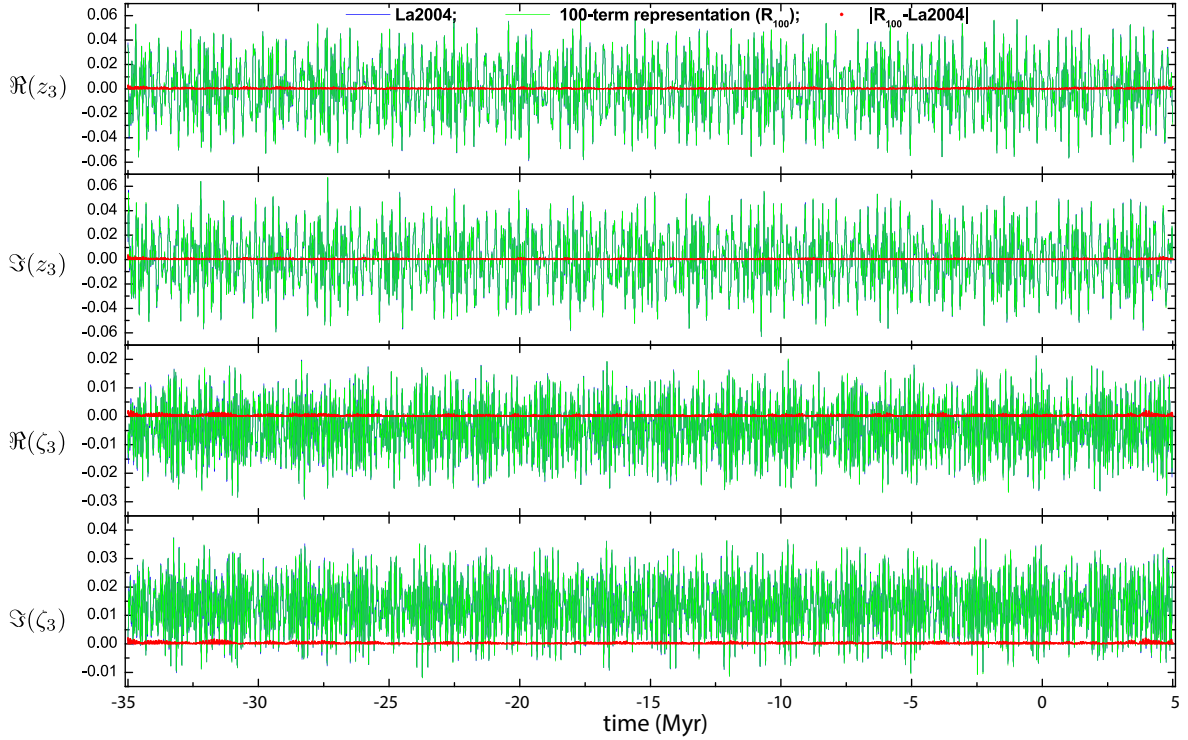
Fig. 11. Comparison between the eccentricity and inclination ephemerides of La2004 and their respective 100-term representations over the time interval from -35 Myr to 5 Myr with origin at J2000. Both representations are in the form of Eq. (31), with the Chebyshev expansions approximating the fundamental frequencies specified in Table A.2, and main frequency index vectors and complex amplitudes of all 100 terms in the full Tables A.3 and A.4 available at the CDS.
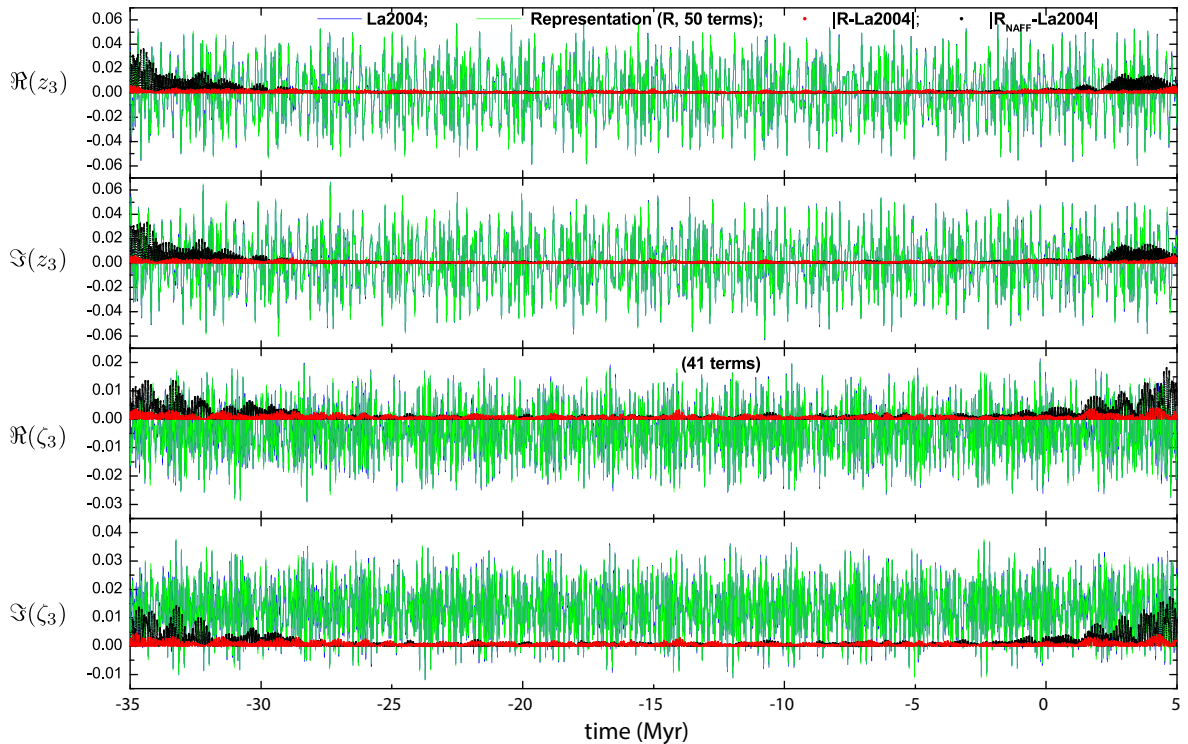
Fig. 12. Comparison between the eccentricity ephemeris z_3 and the inclination ephemeris ζ_3 of La2004 and their respective representations by NAFF ($\mathfrak{R}_{NAFF}$) and by the present algorithms ($\mathfrak{R}$). The number of terms of z_3-representation is 50 for both $\mathfrak{R}_{NAFF}$ and $\mathfrak{R}$, and the number is 41 in the case of ζ_3.

truncation criterion was roughly that the discrepancy in a fundamental frequency should not induce an error in phase larger than $2\pi/10^4$ over several tens of million years.

There are two important libration frequencies, $r_1 = 0.251085$ arcsec yr^{-1} of the resonance argument $2(\varpi_4^\bullet - \varpi_3^\bullet) - (\Omega_4^\bullet - \Omega_3^\bullet)$ and $r_2 = 0.117222$ arcsec yr^{-1} of $2(\varpi_1^\bullet - \varpi_5^\bullet) - (\Omega_1^\bullet - $

$\Omega_2^\bullet$). To include them as additional fundamental frequencies, we expressed the main frequency as

$$\omega = \sum_{i=1}^{8}(m_i g_i + n_i s_i) + \sum_{j=1}^{2} k_j r_j. \quad (30)$$

The d'Alembert characteristic, $\sum_{i=1}^{8}(m_i + n_i) = 1$, was used to exclude non-physical frequency index vectors.

To show to which degree our algorithm is practically useful, we discuss here the following two 100-term representations ($\mathfrak{R}_{100}$ for short),

$$z_3(t) = \sum_{j=1}^{100} a_{\boldsymbol{k}(j)} e^{i\varphi_{\boldsymbol{k}(j)}(t)}, \quad \zeta_3(t) = \sum_{j=1}^{100} b_{\boldsymbol{k}(j)} e^{i\varphi_{\boldsymbol{k}(j)}(t)}, \quad (31)$$

where with $\boldsymbol{f} = (g_1, \ldots, g_8, s_1, \ldots, s_8, r_1, r_2)$ and $\boldsymbol{k} = (m_1, \ldots, m_8, n_1, \ldots, n_8, k_1, k_2)$, the phase increment $\varphi_{\boldsymbol{k}}(t) = \int_0^t \langle \boldsymbol{k}, \boldsymbol{f}(\tau) \rangle d\tau$ is associated with the main frequency $\langle \boldsymbol{k}, \boldsymbol{f} \rangle$. The way the residuals decrease with increasing number of representation terms in the two representation procedures of $\mathfrak{R}_{100}$ is shown in Fig. 10.

The leading 40 terms of these two representations are given in Tables A.3 and A.4, respectively, where the terms are reordered according to their real amplitudes and data are rounded to a convenient number of digits. Comparing these results with those given in Tables 4 and 5 of Laskar (1990), we find that they are coherent with each other in the sense that all the main frequencies explicitly identified previously can be found in our tables.

The full versions of Tables A.3 and A.4 are available at the CDS. They are plain-text tables providing all terms of $\mathfrak{R}_{100}$ in the form of Eq. (31). Together with the data presented in Table A.2 for computing $\boldsymbol{f}$, these two tables can be used to compute the eccentricity and inclination variables from $\mathfrak{R}_{100}$. The errors of $\mathfrak{R}_{100}$ as solution representation are shown in Fig. 11. Based on the information in this figure, we expect that our algorithm should be efficient in producing compact and precise representations of long-term ephemerides of major solar system bodies.

To conclude, we explicitly illustrated the advantage of representing ephemerides by taking into consideration the frequency drifts by comparing the representations given by a direct use of NAFF and the modified present algorithms. The quasi-periodic representations ($\mathfrak{R}_{\text{NAFF}}$ for short) of the same z_3- and ζ_3-

ephemeris given by the standard realization of NAFF, which is a built-in tool of the algebraic system TRIP[5], have 50 and 41 terms, respectively. NAFF does not recover more terms because it encounters a frequency that at a given level of precision is already recovered in a previous step. To more precisely show the advantage of taking frequency drifts into consideration, we produced for z_3 and ζ_3 representations ($\mathfrak{R}$) with the same number of terms as the corresponding $\mathfrak{R}_{\text{NAFF}}$ representation. The comparison between $\mathfrak{R}$ and $\mathfrak{R}_{\text{NAFF}}$ is shown in Fig. 12. This figure clearly shows the improvements brought by introducing frequency drifts into the representation model.

References

Arnol'd, V. I. 1963, Russ. Math. Surv., 18, 9
Bretagnon, P. 1974, A&A, 30, 141
Chapront, J. 1995, A&AS, 109, 181
Fienga, A., Manche, H., Laskar, J., & Gastineau, M. 2008, A&A, 477, 315
Kolmogorov, A. 1954, Dokl. Akad. Nauk. SSSR, 98, 469
Lagrange, J. L. 1782, Oeuvres Complètes, 5, 211
Laskar, J. 1985, A&A, 144, 133
Laskar, J. 1986, A&A, 157, 59
Laskar, J. 1988, A&A, 198, 341
Laskar, J. 1989, Nature, 338, 237
Laskar, J. 1990, Icarus, 88, 266
Laskar, J. 1993, Phys. D, 67, 257
Laskar, J. 1999, Hamiltonian Systems with Three or More Degrees of Freedom, 134
Laskar, J. 2003, ArXiv e-prints [arXiv:math/0305364]
Laskar, J., & Robutel, P. 2001, Celestial Mech. Dyn. Astron., 80, 39
Laskar, J., Froeschlé, C., & Celletti, A. 1992, Phys. D Nonlinear Phenom., 56, 253
Laskar, J., Robutel, P., Joutel, F., et al. 2004, A&A, 428, 261
Laskar, J., Fienga, A., Gastineau, M., & Manche, H. 2011, A&A, 532, A89
LeVerrier, U. 1840, Additions à la Connaissance des temps pour l'an 1843 (Paris: Bachelier), 3
LeVerrier, U. 1841, Additions à la Connaissance des temps pour l'an 1843 (Paris: Bachelier), 28
Milankovitch, M. 1941, Kanon der Erdbestrahlung und seine Anwendung auf das Eiszeitenproblem (Belgrade: Spec. Acad. R Serbe)
Moser, J. K. 1962, Nach. Akad. Wiss. Göttingen, Math. Phys., II, 1
Quinn, T. R., Tremaine, S., & Duncan, M. 1991, ApJ, 101, 2287
Sussman, G. J., & Wisdom, J. 1992, Science, 257, 56

---

[5] http://www.imcce.fr/trip/

Appendix A: Chebyshev polynomials and coefficients for the La2004 solution

Table A.1. Expressions of the Chebyshev polynomials up to degree 15.

m	$T_m(x)$
0	1
1	x
2	$2x^2 - 1$
3	$4x^3 - 3x$
4	$8x^4 - 8x^2 + 1$
5	$16x^5 - 20x^3 + 5x$
6	$32x^6 - 48x^4 + 18x^2 - 1$
7	$64x^7 - 112x^5 + 56x^3 - 7x$
8	$128x^8 - 256x^6 + 160x^4 - 32x^2 + 1$
9	$256x^9 - 576x^7 + 432x^5 - 120x^3 + 9x$
10	$512x^{10} - 1280x^8 + 1120x^6 - 400x^4 + 50x^2 - 1$
11	$1024x^{11} - 2816x^9 + 2816x^7 - 1232x^5 + 220x^3 - 11x$
12	$2048x^{12} - 6144x^{10} + 6912x^8 - 3584x^6 + 840x^4 - 72x^2 + 1$
13	$4096x^{13} - 13312x^{11} + 16640x^9 - 9984x^7 + 2912x^5 - 364x^3 + 13x$
14	$8192x^{14} - 28672x^{12} + 39424x^{10} - 26880x^8 + 9408x^6 - 1568x^4 + 98x^2 - 1$
15	$16384x^{15} - 61440x^{13} + 92160x^{11} - 70400x^9 + 28800x^7 - 6048x^5 + 560x^3 - 15x$

A.1. Chebyshev polynomials

Chebyshev polynomials as defined by the recurrence relation

$$
\begin{aligned}
&T_0(x) = 1, \quad T_1(x) = x \qquad (-1 \le x \le 1) \\
&T_{m+1}(x) = 2xT_m(x) - T_{m-1}(x) \quad (m > 1)
\end{aligned}
\tag{A.1}
$$

form a non-normalized but orthogonal basis under the inner product

$$
\langle f(x), g(x) \rangle = \int_{-1}^{1} \frac{f(x)g(x)}{\sqrt{1-x^2}} \mathrm{d}x. \tag{A.2}
$$

This can be easily checked by straightforward calculations

$$
\langle T_i(x), T_j(x) \rangle = \int_{-1}^{1} \frac{T_i(x)T_j(x)}{\sqrt{1-x^2}} \mathrm{d}x = \begin{cases} \pi & (i = j = 0) \\ \pi/2 & (i = j \ne 0) \\ 0 & (i \ne j). \end{cases} \tag{A.3}
$$

Their linear combination, called Chebyshev expansion, is often used to approximate a function $h(x)$ defined on $[-1, 1]$

$$
h(x) \approx h_c(x) = \sum_{m=0}^{M} c_m T_m(x), \tag{A.4}
$$

where

$$
c_m = \begin{cases} \frac{1}{\pi} \langle h(x), T_m(x) \rangle & (m = 0) \\ \frac{2}{\pi} \langle h(x), T_m(x) \rangle & (m \ne 0). \end{cases} \tag{A.5}
$$

The indefinite integral of the Chebyshev expansion $h_c(x)$ writes, up to an arbitrary constant,

$$
H_c(x) = \sum_{m=1}^{M+1} C_m T_m(x), \tag{A.6}
$$

where, with $c_{M+1} = c_{M+2} = 0$,

$$
C_m = \begin{cases} \frac{2c_0 - c_2}{2} & (m = 1), \\ \frac{c_{m-1} - c_{m+1}}{2m} & (m = 2, \dots, M+1). \end{cases} \tag{A.7}
$$

A.2. Coefficients for the Earth La2004 solution

Here we provide the tables of coefficients used for the representation of the Earth La2004 eccentricity and inclination solution over the interval $[-35\,\mathrm{Myr}: +5\,\mathrm{Myr}]$ (Laskar et al. 2004).

Table A.2. Coefficients of Chebyshev expansion $\sum_m c_m T_m$ approximating the major fundamental frequencies $(g_1, \ldots, g_8, s_1, \ldots, s_8)$ (arcsec yr^{-1}) of the solar system over the time interval from -35 Myr to 5 Myr with origin at J2000.

	m	c_m		m	c_m
g_1	0	5.59436858	s_1	0	−5.61412432
	1	−0.02916946		1	0.01897975
	2	0.00259949		2	0.00616405
	3	−0.00858191		3	−0.00967633
	4	−0.00538351		4	−0.00048289
	5	−0.00216691		5	−0.00405450
	6	−0.00311006		6	−0.00319098
	7	0.00137912		7	0.00116236
	8	−0.00225709		8	−0.00048593
	9	0.00318074		9	0.00207233
	10	0.00431717		10	0.00194425
	11	−0.00288184		11	−0.00103824
	12	−0.00189708		12	−0.00117501
	13	0.00127879		13	0.00006311
	14	0.00065723		14	0.00030964
	15	−0.00017362		15	−0.00037496
g_2	0	7.45660678	s_2	0	−7.07313208
	1	−0.00276205		1	0.04218433
	2	0.00177713		2	−0.00001315
	3	0.00056064		3	−0.00225169
	4	−0.00002096		4	0.00386256
	5	0.00090782		5	−0.00280878
	6	0.00096229		6	0.00247914
	7	−0.00024908		7	0.00109449
	8	0.00042855		8	−0.00064733
	9	−0.00071228		9	0.00229722
	10	−0.00091971		10	−0.00000725
	11	0.00061668		11	−0.00193901
	12	0.00047006		12	0.00088350
	13	−0.00024111		13	0.00053257
	14	−0.00015053		14	0.00024897
	15	0.00007778		15	0.00024128
g_3	0	17.36445990	s_3	0	−18.84810087
	1	0.01585020		1	−0.00165582
	2	−0.00496995		2	0.00007105

Notes. Also listed are the used constant libration frequencies r_1 and r_2 (arcsec yr^{-1}).

Table A.2. continued.

	m	c_m		m	c_m
	3	0.00540088		3	−0.00140634
	4	0.00496032		4	0.00050744
	5	−0.00226103		5	0.00039039
	6	−0.00004476		6	0.00135948
	7	0.00006943		7	0.00065306
	8	0.00007190		8	−0.00041702
	9	−0.00037475		9	−0.00026792
	10	−0.00059252		10	−0.00018687
	11	0.00025574		11	0.00004492
	12	0.00035119		12	0.00013288
	13	−0.00020600		13	0.00001794
	14	−0.00000042		14	−0.00005746
	15	0.00011279			
g_4	0	17.91086281	s_4	0	−17.75496646
	1	0.02044603		1	0.00670633
	2	−0.00851446		2	−0.00717162
	3	0.00812180		3	0.00313019
	4	0.00866961		4	0.00807398
	5	−0.00482118		5	−0.00498282
	6	−0.00137335		6	−0.00116638
	7	0.00011721		7	0.00058378
	8	0.00083465		8	0.00021726
	9	−0.00041179		9	0.00016650
	10	−0.00109334		10	−0.00060643
	11	0.00069484		11	0.00014173
	12	0.00045529		12	0.00039520
	13	−0.00029042		13	−0.00024600
	14	−0.00014170		14	−0.00006598
	15	0.00008189		15	0.00012665
g_5	0	4.25745185	s_5	0	0.00000015
g_6	0	28.24498422	s_6	0	−26.34785292
	1	0.00010582		1	0.00000053
	2	0.00011695		2	−0.00000514
	3	−0.00002698			
	4	−0.00001157			
g_7	0	3.08795246	s_7	0	−2.99252583
	1	−0.00000017			
g_8	0	0.67302182	s_8	0	−0.69173649
				1	0.00000001
r_1	0	0.251085	r_2	0	0.117222

Table A.3. Leading 40 terms of the 100-term representation $z_3(t)$, as expressed in Eq. (31).

No.	$\langle k, f \rangle$	$\text{Abs}(a_k) \times 10^6$	$\text{Arg}(a_k)$ (degree)
1	g_5	18984	-68.812
2	g_2	16088	95.535
3	g_4	13041	17.345
4	g_3	9042	-54.984
5	g_1	4314	-175.273
6	$g_4 - r_1$	2583	-92.093
7	$g_3 - r_1$	2415	15.391
8	$g_3 + r_1 + r_2$	2377	-136.939
9	$g_4 + s_3 - s_4$	1934	-128.504
10	g_6	1498	160.676
11	$2g_1 - g_5$	1393	82.417
12	$g_3 + g_4 - g_6$	1372	178.968
13	$g_1 - r_2$	1298	140.905
14	$g_3 - s_3 + s_4$	1282	-87.475
15	$g_2 - r_2$	1156	-127.879
16	$g_4 - 2r_1$	1153	15.739
17	$g_1 + r_2$	1085	49.430
18	$g_2 - g_3 + g_6 - r_2$	1028	-40.633
19	$g_4 - r_2$	946	149.088
20	$g_2 + r_2$	942	123.828
21	$-g_1 + 2g_4 - g_5 + s_3$	916	82.353
22	$-g_3 + 2g_4 - 2r_1$	903	63.075
23	$g_3 + s_3 - s_4$	824	150.057
24	$g_3 + 2r_1$	816	145.441
25	$g_4 + r_1$	806	165.483
26	$g_4 + s_3 - s_4 - r_1$	756	113.428
27	$g_1 - s_3 + s_4 + r_2$	712	-121.353
28	$g_4 - s_3 + s_4$	697	-14.943
29	$2g_3 - g_4 + 2r_2$	605	-21.586
30	g_7	577	-146.073
31	$g_4 + r_2$	573	52.634
32	$g_3 + r_2$	504	-21.947
33	$g_1 + g_5 - g_7 + r_1$	432	152.449
34	$-g_1 + g_2 + g_5 - r_2$	383	-28.070
35	$g_3 + r_1$	275	-4.253
36	$g_3 - r_2$	144	89.319
37	$g_2 - r_1 - r_2$	121	-36.562
38	$g_2 - r_1 + r_2$	104	-105.175
39	$-g_1 + g_4 + g_5$	92	-173.117
40	$g_1 - r_1$	87	99.123

Notes. The full table is available at the CDS.

Table A.4. Leading 40 terms of the 100-term representation $\zeta_3(t)$, as expressed in Eq. (31).

No.	$\langle k, f \rangle$	$\text{Abs}(b_k) \times 10^6$	$\text{Arg}(b_k)$ (degree)
1	s_5	13774	107.587
2	s_3	8666	-62.318
3	s_4	4647	96.756
4	s_1	4085	27.817
5	s_2	3312	80.364
6	$g_3 - g_4 + s_4$	2745	-167.132
7	$s_2 + 2r_2$	2041	-44.496
8	$s_2 + r_2$	1543	125.410
9	$g_3 - g_4 + s_3$	1530	-137.669
10	$s_1 + s_3 - s_4 - r_2$	1469	91.798
11	$s_2 - r_2$	1450	23.071
12	$s_1 + r_2$	1417	-116.942
13	s_6	1333	110.029
14	s_7	889	9.186
15	$s_2 + r_1$	646	-50.277
16	s_8	641	26.053
17	$s_3 - r_1$	613	-178.905
18	$s_1 + s_3 - s_4$	532	-177.568
19	$s_1 - 2r_2$	518	101.955
20	$s_3 - r_2$	484	106.762
21	$g_3 - g_4 + s_3 + r_1$	481	-21.125
22	$g_3 - g_4 + s_2 + r_1$	445	-5.831
23	$s_2 - s_3 + s_4$	364	72.700
24	$s_2 - s_3 + s_4 - r_2$	344	31.282
25	$s_2 - r_1$	341	20.734
26	$s_2 - 2r_2$	320	-51.578
27	$g_3 - g_4 + s_1$	315	-118.127
28	$g_3 - s_1 + s_6 + s_7 - s_8$	304	172.667
29	$s_1 - r_1$	293	149.314
30	$-s_4 + s_6 - s_7 + 2s_8$	293	-76.858
31	$s_1 + 2r_1 - r_2$	292	134.167
32	$-g_3 + s_5 + s_8 + r_1$	285	-170.886
33	$-g_3 + g_4 + s_2$	268	47.758
34	$-g_3 + g_4 + s_2 - r_2$	258	-27.836
35	$-g_3 + g_4 + s_4$	244	-18.592
36	$g_4 + s_6 - s_8 + r_1$	230	109.121
37	$g_3 - g_4 + s_4 - r_1$	221	-91.732
38	$s_2 + s_5 - s_8 - 2r_1$	217	173.446
39	$-g_3 + g_4 + s_2 - r_1$	198	24.257
40	$s_1 + 2r_1$	78	77.412

Notes. The full table is available at the CDS.